Available online at www.sciencedirect.com
ScienceDirect
Nuclear Instruments and Methods in Physics Research A 565 (2006) 543–550
NUCLEAR INSTRUMENTS & METHODS IN PHYSICS RESEARCH Section A
www.elsevier.com/locate/nima

The timing system for the CDF electromagnetic calorimeters

M. Goncharov[a], T. Kamon[a], V. Khotilovich[a], V. Krutelyov[a], S.W. Lee[a], D. Toback[a,*], P. Wagner[a], H. Frisch[b], H. Sanders[b], M. Cordelli[c], F. Happacher[c], S. Miscetti[c], R. Wagner[d]

[a]*Texas A&M University, USA*
[b]*University of Chicago, USA*
[c]*INFN-Frascati, Italy*
[d]*Argonne National Laboratory, USA*

Received 15 December 2005; received in revised form 30 May 2006; accepted 2 June 2006
Available online 30 June 2006

Abstract

We report on the design and performance of the electromagnetic calorimeter timing readout system (EMTiming) for the Collider Detector at Fermilab (CDF). The system will be used in searches for rare events with high-energy photons to verify that the photon is in time with the event collision, to reject cosmic-ray and beam-halo backgrounds, and to allow direct searches for new, heavy, long-lived neutral particles that decay to photons. The installation and commissioning of all 862 channels were completed in Fall 2004 as part of an upgrade to the Run II version of the detector. Using in situ data, including electrons from $W \to e\nu$ and $Z \to ee$ decays, we measure the energy threshold for a time to be recorded to be 3.8 ± 0.3 GeV (1.9 ± 0.1 GeV) in the central (plug) portion of the detector. Similarly, for the central (plug) portion we measure a timing resolution of 600 ± 10 ps (610 ± 10 ps) for electrons above 10 GeV (6 GeV). There are very few system pathologies such as recording a time when no energy is deposited, or recording a second, fake time for a single energy deposit.

PACS: 07.50.Qx; 29.40.Vj; 29.40.Mc

Keywords: Electromagnetic calorimeter; Timing; CDF

1. Introduction

Timing readout for the electromagnetic (EM) calorimeters [1,2] was recently installed as part of an upgrade to the Run II version of the Collider Detector at Fermilab (CDF) [3]. This system, known as EMTiming [4], is similar to the existing hadronic calorimeter system [5] but has a resolution of less than a nanosecond and covers the central (CEM, $|\eta| < 1.1$) and plug (PEM, $1.1 < |\eta| < 2.1$) portions of the calorimeter, where $\eta = -\ln \tan(\theta/2)$, and θ is the angle from the beamline.

The design of the EMTiming system is optimized for searches for production of new particles that decay into high-energy photons as would be the case in some models of Supersymmetry or Large Extra Dimensions [6]. Final state particles from proton–anti-proton collisions traverse the CDF detector and the EMTiming system records the time of arrival for those that deposit large amounts of energy in the EM calorimeter. To improve the search sensitivity and robustness, the system can verify that all photons (or other energy) are from the primary collision [7] and reject and estimate the rate of cosmic-ray and beam-related backgrounds. In addition, the system allows for a new class of searches for heavy, long-lived neutral particles that decay to photons and arrive at the calorimeter with a time that is delayed relative to expectations [8].

In the following sections we describe the various components of the EMTiming system and the system performance from its first four months of operation. In Sections 2–4 we give an overview of the system and describe the path of the

*Corresponding author. Tel.: +1 979 845 1179; fax: +1 979 845 2590.
E-mail address: toback@tamu.edu (D. Toback).

0168-9002/$ - see front matter © 2006 Published by Elsevier B.V.
doi:10.1016/j.nima.2006.06.011

calorimeter signals through the various components in the system, with particular emphasis on the differences between the CEM and PEM systems which were originally built with different readout. In Section 5 we describe the system performance as measured using collision data in situ.

2. Overview of the system

Particles from the collision that shower and deposit energy in the EM calorimeters create light within the scintillators [1,2] that can be used for a timing measurement. Photo-multiplier tubes (PMTs) collect this light and convert the particle energy into an electrical signal. Prior to the installation of the EMTiming system this signal was only used as part of the energy measurement. The EMTiming system, shown schematically in Fig. 1, routes a copy of the PMT signal to a passive Transition Board (TB) and Amplifier–Shaper–Discriminator (ASD) board pair that, in turn, sends its signal to a Time-to-Digital Converter (TDC) board for a timing measurement.

The design takes into account the differences between the existing CEM and PEM readout sub-systems while trying to make the overall system as uniform and modular as possible. While the PEM, assembled for the beginning of Run II, was designed with a timing upgrade in mind, the CEM was not. In Section 3 we describe the differences between the PMT outputs for the CEM and PEM, and the designs used to get a timing signal out of the PMTs and onto the ASD boards. In Section 4 we describe the boards that collect the signals from the PMTs, amplify, shape, combine and use them as input to the discriminator, and output the results to a TDC. Table 1 provides a summary of the system specifications.

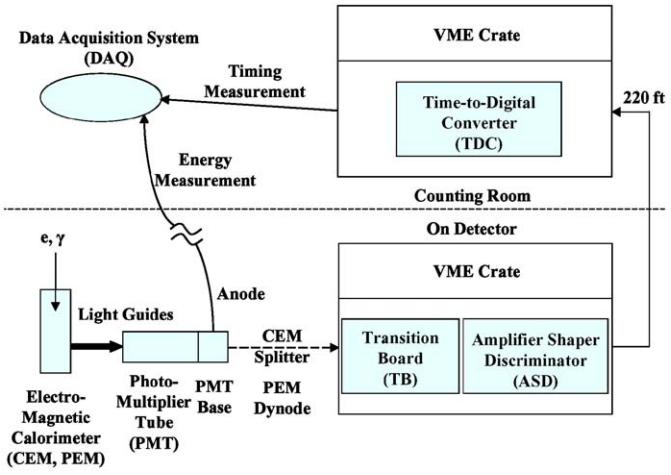

Fig. 1. A schematic diagram of the EMTiming system hardware on the CDF detector. Note that the CEM PMTs use "splitter" outputs (described in Section 3) to send their signals to the discriminators through transition boards, while the PEM uses dynode outputs.

Table 1
Overview of the EMTiming system hardware and performance

	CEM	PEM
Coverage	$\|\eta\| < 1.1$	$1.1 < \|\eta\| < 2.1$
PMT	Hamamatsu R580	Hamamatsu R4125
Physical tower segmentation	$\Delta\phi = 15^\circ$, $\Delta\eta \approx 0.1$	$\Delta\phi = 7.5^\circ$, $\Delta\eta \approx 0.1$
Tower readout	2 PMTs per tower	1 PMT per tower
PMT→ ASD readout method	Analog splitter, both PMTs from a single tower combined	Dynode, PMTs from two adjacent towers, in $\Delta\phi$, combined
Total number of PMTs/ASD channels	956/478	768/384
Number of TB/ASD/TDC boards	32/32/8	16/16/4
Energy threshold (50% efficiency point)	3.8 ± 0.3 GeV	1.9 ± 0.1 GeV
Threshold width	1.4 ± 0.2 Gev	0.6 ± 0.1 GeV
Timing resolution at asymptotic energies	600 ± 10 ps	610 ± 10 ps

Note that the calorimeter is physically segmented into 1246 "towers," and that each timing channel consists of two input PMTs for each ASD/TDC output line. As described in Section 5.1 the efficiency for a time to be recorded is energy dependent and is well described by an efficiency plateau, threshold and width. All channels have a plateau that is $\approx 100\%$ efficient, and the uncertainties listed for the threshold and width values represent the channel-to-channel variation in the system. As described in Section 5.2 the timing resolution asymptotically improves as a function of energy, and the numbers quoted here are for energies above 10 and 6 GeV for the CEM and PEM, respectively; above these values the resolution is constant within errors. For more details on the CEM and PEM calorimeters see Refs. [1,2].

3. The CEM and PEM PMT output signals

As described in Table 1, the CEM and PEM have different designs and PMT readout schemes. In the CEM, the original PMT bases are custom designed[1] and only provide an anode output via a LEMO connector. In the PEM, the system was designed with the dynode signal already available using AMP connector units. The rise times of the PMT output signals, as measured from 10% of the voltage-max to 90% of the voltage-max, are ≈ 10 ns and 6 ns for the CEM and PEM, respectively.

In order to continue to use the pre-existing CEM hardware, we designed an inductive signal "splitter" board that is placed between the PMT base and the original 25 ft RG174 cable that carries the anode signal for an energy measurement. The splitter routes a fraction of the PMT pulse energy for timing use, while not affecting the energy measurement. As shown in Fig. 2 the anode cable is connected, via a LEMO connector, to a printed circuit board where the primary and shield wires are separated. The primary line is then passed through a small circular

[1]We note that these bases were built almost 20 years prior to the EMTiming installation, and are largely unmodified since then.

ferrite after which the wires are rejoined. A secondary wire is wound around the ferrite so that a signal from the PMT anode induces a voltage for timing use. This secondary signal is sent via an RG174 cable with a length that varies between 23 and 36 ft to the TBs depending on the PMT location on the detector. The splitter solution avoids potential ground-loop problems since there is no electrical contact between the timing and energy readout lines. All cables have LEMO connectors on each end to facilitate installation.

The secondary pulse used for the timing measurement has a voltage that is 15% of the primary signal. Since the two lines are only inductively coupled, and the energy measurement is done with a charge integration device [9], in principle this solution should not affect the energy measurement since no charge can be lost. In order to verify this, test-stand comparisons of the integrated charge for a PMT pulse, with and without a splitter, were performed at various points over the full energy integration range. There was no observed (systematic or otherwise) effect on the linearity or resolution for any energy, with a measurement uncertainty of approximately 10% of the 1σ variation in the charge-integration measurement itself (for a given energy).

The PEM was designed with a potential timing upgrade in mind. The dynode outputs from each PMT are collected in groups of 16 and made available for connection via off-the-shelf AMP connectors. The individual dynode outputs are then sent via 25 ft RG174 cables to the TBs and connected via LEMO connectors.

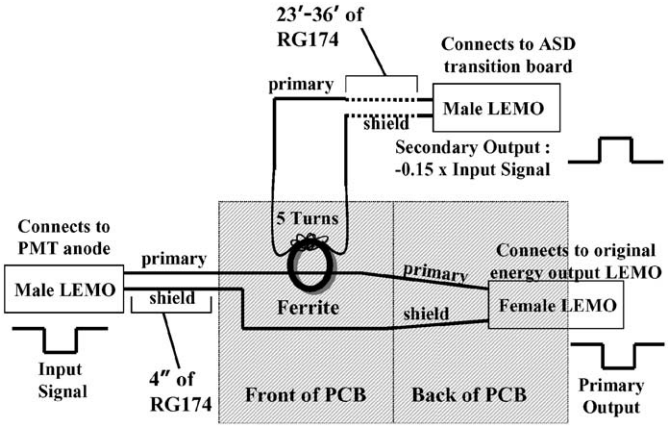

Fig. 2. An electronics schematic for the "splitter" printed circuit board (PCB) used in the CEM timing measurement. Note that RG174 refers to the coaxial cable used in the system. The primary output is used for the energy measurement while the secondary output is used for the timing measurement and is the input to the transition boards.

4. Signal discrimination and transfer to the TDC

Beyond the inputs to the TBs the remaining system components (TBs, ASDs, the long cables and TDCs) are identical for the CEM and PEM. Each component is designed for low cost and large numbers of channels per board/cable without compromising the timing resolution. The number of boards for each sub-system is summarized in Table 1.

Each TB is capable of receiving cables from 48 PMTs. As shown in Fig. 3, processing begins with an *RC* circuit and a transformer. The *RC* circuit helps reduce reflections back to the PMT that might otherwise cause a second, erroneous signal to be sent, and the transformer helps reduce ground-loop or potential DC-offset problems that might give rise to spurious signals when no energy is deposited. Each line is passed, via the crate backplane, to the ASD.

On the ASD the signals from two PMTs are summed and compared to a threshold with the digital result being sent to the TDC. As shown on the right-hand side of Fig. 3, each PMT signal is amplified, then combined in an analog sum with a threshold offset, and sent to a comparator. This operates as a fixed-threshold discriminator with a 2 mV

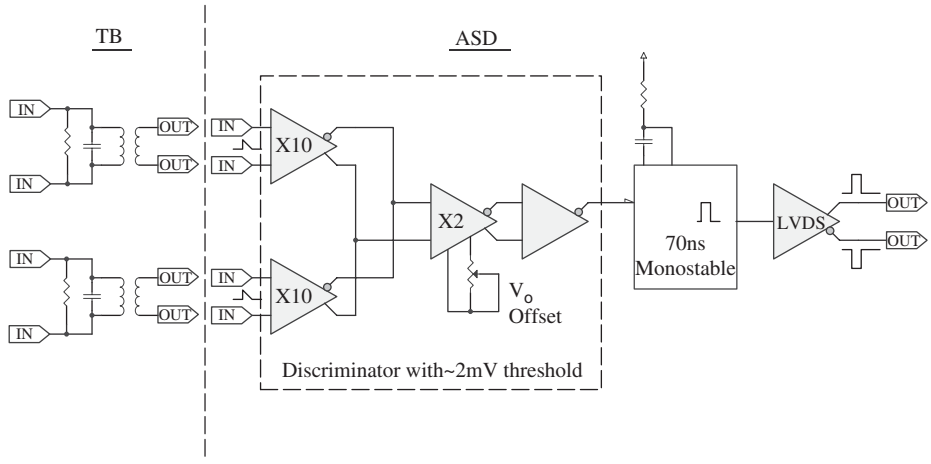

Fig. 3. A schematic for the signal processing that occurs on the Transition Board (TB) and Amplifier-Shaper-Discriminator board (ASD). The *RC* circuit ($R = 150\,\Omega$, $C = 12$ pF) in parallel with a transformer (1:1) on the TB is designed to reduce noise and reflection problems at the input ($Z = 50\,\Omega$). On the ASD the amplifiers and comparator sum the two PMT signals and discriminate on the leading edge with a 2 mV threshold.

threshold. The resulting signal triggers a monostable with an output width of 70 ± 10 ns that in turn feeds a National Semiconductor DS90C031 LVDS driver.

The output for each channel on an ASD board is placed on a single 220 ft multi-wire twisted-pair cable (3M 3644B/50) that goes from the collision hall calorimeter crates, upstairs to the TDCs. At this length these cables have a rise time of ~50 ns. However, test-bench studies show that as long as the input LVDS signal width is >50 ns, then we expect negligible data-transfer loss and timing jitter of <30 ps. The receiver chip set is located on one of the standard CDF 96 channel TDCs [10] that are a part of the data acquisition system (DAQ) and read out for each event.

5. System performance

The EMTiming system operates at CDF when the Tevatron is in Collider mode. During data taking, protons and anti-protons collide every 396 ns, on average, at the center of the detector. The variation in the time and position of the collision is $\sigma_{\text{time}} \approx 1.3$ ns and $\sigma_{\text{position}} \approx 25$ cm, respectively. The typical time of flight from the collision point to the calorimeter is 5 ns and has an RMS variation of about 0.6 ns. If there is enough energy deposited, the TDC will record a time of arrival and this time is straightforwardly corrected for each of the above, and other, effects.

The system operation can be described in terms of its efficiency to record a time, the timing resolution and the rate of spurious hits. We study the performance in situ using collisions that produce hadrons from jet events, and electrons from $Z \rightarrow ee$ and $W \rightarrow e\nu$ events. The results presented here represent the data taken during the first four months of Tevatron running in 2005.

5.1. System efficiency

The efficiency, the ratio of numbers of events with a time recorded in the TDC to all events, is a strong function of the

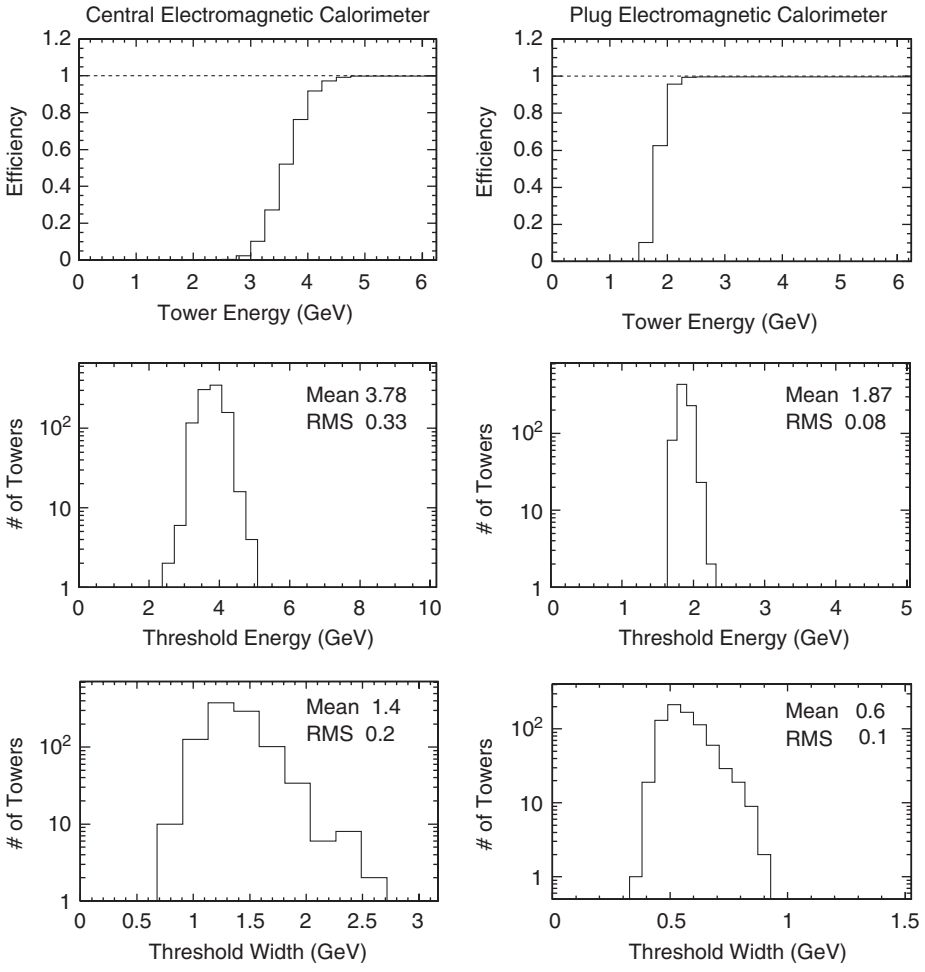

Fig. 4. The EMTiming system response as a function of the energy deposited in the EM calorimeter for a sample of hadrons from jets measured in the detector. The top plots show the efficiency (the fraction of the numbers of events with a time recorded in the TDC to all events) as a function of the energy for the CEM and PEM, and includes all channels. The bottom two rows show histograms of the energy threshold and threshold width of the individual channels and indicate the uniformity of the system.

PMT output signal size and is thus energy dependent. The efficiency as a function of the energy deposited in the tower is shown in the top part of Fig. 4 for the CEM and PEM separately, and includes all towers together. The distribution is well described by an error/smeared step function, $\mathrm{Erf}(E_{\mathrm{th}}, \sigma, \varepsilon)$, where E_{th} is the threshold, σ is the transition width at threshold, and ε is the plateau efficiency. We investigated each fully instrumented tower separately and found that the efficiency plateaus at 100% and, as shown in the bottom parts of Fig. 4, that the threshold and width values, as determined from a fit, are 3.8 ± 0.3 GeV (1.9 ± 0.1 GeV) and 1.4 ± 0.2 GeV (0.6 ± 0.1 GeV), respectively, in the CEM (PEM) calorimeters, respectively.

5.2. Timing corrections and system resolution

The time of arrival recorded by the TDC is a "raw" time and has an 8 ns variation due to different effects. We take into account the dominant effects to produce a "corrected time" distribution that is centered at 0 ns for relativistic particles that are produced promptly in the collision [4]. The corrected time is given by

$$t_{\mathrm{corrected}} = t_{\mathrm{Raw}} + C_{\mathrm{Start}} + C_{\mathrm{Energy}} + C_{\mathrm{Energy\ Asymmetry}} - C_{\mathrm{Time\ of\ Flight}} - C_{\mathrm{Collision\ Time}} \quad (1)$$

where the corrections are described below and determined on a tower-by-tower basis, unless otherwise noted, using in situ data:

- There is a constant offset between the average time of arrival of the energy deposited in the calorimeter and the TDC-start from the DAQ. This constant, C_{Start}, is dominated by the overall cable lengths and thus can vary greatly from tower to tower.
- Since the ASDs use a fixed-threshold discrimination method, the PMT pulse shape produces a "slewing" that makes the recorded time energy dependent. We use a set of empirically derived constants given by

$$C_{\mathrm{Energy}} = \frac{A_1}{\ln(x)} + \frac{A_2}{x^2} \quad (2)$$

  where A_1 and A_2 are constants and x is the sum of the energies from the two PMTs, as measured in the calorimeter.
- PMT energy response differences as well as the location within a tower where the particle hits can also affect the measured time of arrival. We correct for both effects by taking into account the energy asymmetry between the towers. We use the empirically derived functional form:

$$C_{\mathrm{Energy\ Asymmetry}} = B_0 + B_1 \cdot y + B_2 \cdot y^2 \quad (3)$$

  where B_0, B_1 and B_2 are constants and y is the energy asymmetry of the two PMTs. After the above corrections the timing distribution is Gaussian with an RMS of 1.6 ns.
- The arrival time is corrected for the expected time of flight, $C_{\mathrm{Time\ of\ Flight}}$, using the measured collision position from the tracking chamber [11] and the known calorimeter tower position.
- Finally, the measured collision time, $C_{\mathrm{Collision\ Time}}$, as measured by the tracking chamber [11], is subtracted off on an event-by-event basis.

The system resolution is measured in two ways. Using $Z \to ee$ events we subtract the corrected times of the two electrons, thus canceling the collision time and reducing any other global event mismeasurements effects. The result is shown in Fig. 5 for combinations of electrons in the CEM–CEM, CEM–PEM and PEM–PEM, respectively. The RMS per electron is 600 ± 10 and 610 ± 10 ps for the CEM and PEM, respectively, and is consistent between the measurements. This includes the irreducible TDC resolution of 288 ps (the TDC has a 1 ns binning output, which corresponds to an RMS of $1\,\mathrm{ns}/\sqrt{12} = 288$ ps) as well as a negligible contribution to the uncertainty on $C_{\mathrm{Time\ of\ Flight}}$ from the vertex position measurement.

Fig. 6 shows the timing resolution as estimated from a higher-statistics sample of $W \to e\nu$ events where the time and position of the collision is measured, and corrected for, directly. While the results are consistent with the distributions in Fig. 5 and show that the timing measurement is well described by a Gaussian even out to roughly 5σ for the CEM, a few notes are in order to explain some of the differences. The RMS of the distributions are slightly larger as they include the resolution of the collision-time measurement that is slightly larger for the PEM than for the CEM. In the CEM distribution, top of Fig. 6, we only consider events where the position and time of the origin of the electron track is consistent, within resolution, having come from the measured collision.[2] Unfortunately, a timing measurement for the electron track is not possible in the tracking chamber for the region covered by the PEM. In the case where there are two or more reconstructed collisions in the event that occur at the same position but well separated in time, we cannot use the electron tracking to distinguish which is the correct one. This inability to determine the correct collision from the tracking alone is shown in the bottom part of Fig. 6 as a second Gaussian in the distribution. This second Gaussian corresponds, in this case, to 4% of the events, but should be sample dependent, and has an RMS that reflects the association of the time of arrival with a random collision time. We note that assuming that the energy deposit is from a particle(s) promptly produced at the collision, the measured arrival time can be used to probabilistically help select the proper collision in multi-collision events at high luminosity.

Fig. 7 shows the single tower energy resolution (convolved with the collision-time resolution as in Fig. 6) as measured from a mixed sample of jets and electrons. While the resolution is slightly worse for low energies, the asymptotic resolution stabilizes at energies

[2] We note that we ignore the electron track in our collision measurement so that our results are applicable for photons.

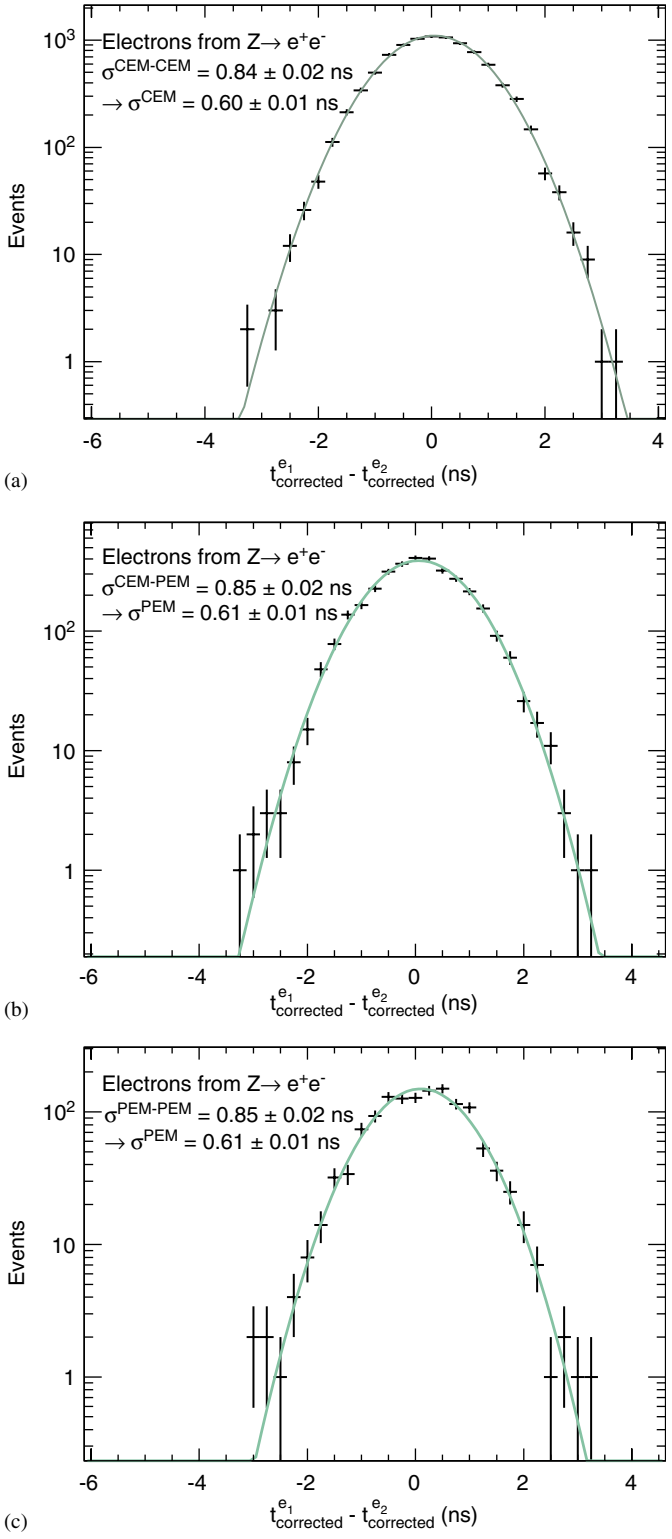

Fig. 5. The difference between the measured times of two electrons from three different samples of $Z \rightarrow ee$ events (CEM–CEM, CEM–PEM and PEM–PEM from top to bottom, respectively). The CEM and PEM resolutions can be determined by taking the RMS/$\sqrt{2}$ which gives single-electron resolutions of 600 ± 10 and 610 ± 10 ps, respectively.

just above 10 and 6 GeV in the CEM and PEM, respectively, to values that are very close to the electron resolution from W's.

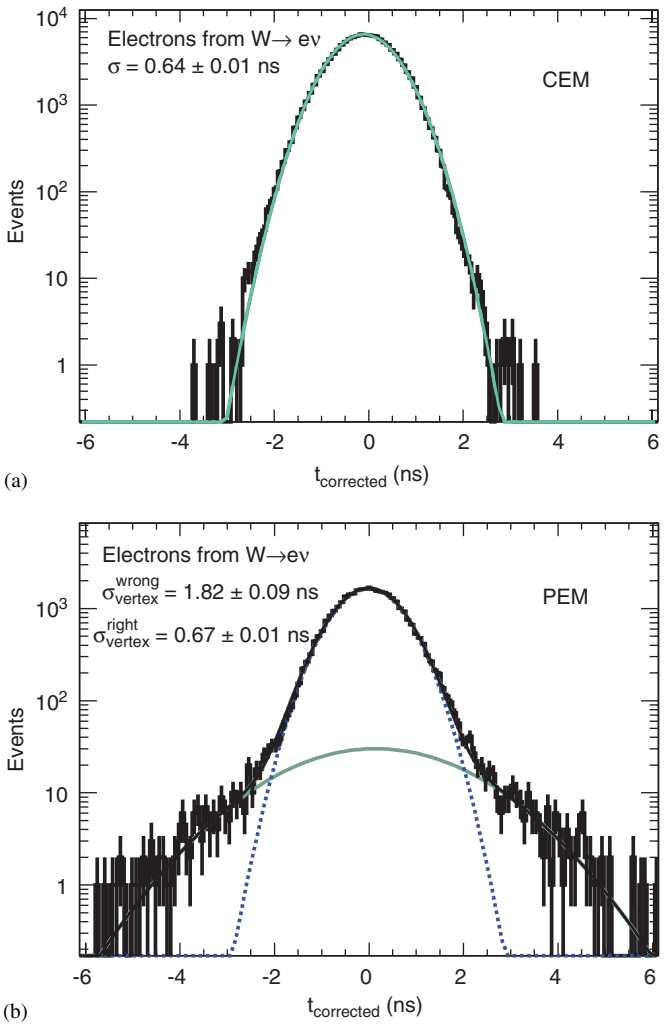

Fig. 6. The timing resolution for single electrons as measured with a sample of $W \rightarrow e\nu$ events. Note that the RMS of these distributions is slightly larger than in Fig. 5 as it includes the resolution of the collision time measurement that is different in the CEM and PEM. As discussed in the text, the second Gaussian in the PEM distribution corresponds to cases where there is a second collision in the event that was incorrectly selected as the event collision time.

5.3. Spurious hits

Finally, we note the rate of spurious hits. We measure the rate at which the system records a time when there is no energy recorded (the fake rate) by the DAQ to be typically less than one occurrence in 10^8 collisions, per tower. We note however that this rate can rise to one in 10^7 if we allow cases where there is some evidence that the energy is not properly read out by the DAQ. The rate at which multiple times are recorded for a single energy deposit, presumably from reflections, is roughly the same as the fake rate, but can be as high as one in 10^5 collisions for a few (<10) towers. However, this is easily corrected for in the final data analysis.

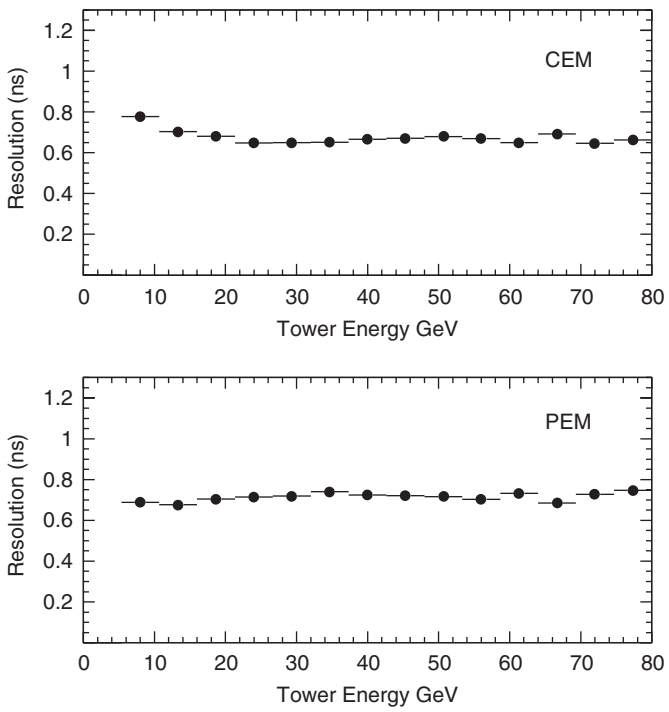

Fig. 7. The timing resolution as a function of energy. Note that the resolution, as in Fig. 6, contains a contribution from the uncertainty in the collision time that is different for the CEM and PEM. In each case the asymptotic value is the same as the electron resolution in Fig. 6.

6. Conclusions

The EMTiming system provides timing readout for the CDF EM calorimeters with good uniformity and resolution. It has its 50% efficiency points at 3.8 ± 0.3 and 1.9 ± 0.1 GeV in the CEM and PEM, respectively, and is 100% efficient well above threshold. After a full set of corrections we find 600 ± 10 and 610 ± 10 ps timing resolutions, respectively, with only small deviations from a Gaussian distribution. There are very few pathologies observed in the data such as recording a time when no energy is deposited or recording multiple times for a single energy deposit. The system is well understood and ready for searches for new particles that decay to photons.

Acknowledgments

The authors would like to acknowledge a number of people who contributed significantly to the EMTiming system. They include Dervin Allen, Chris Battle, Myron Campbell, Matt Cervantes, Steve Chappa, Jamie Grado, Bob DeMaat, Camille Ginsburg, Eric James, Min-Jeong Kim, Steve Kuhlmann, Jonathan Lewis, Mike Lindgren, Pat Lukens, Lew Morris, Peter Onyisi, Steve Payne, Fotis Ptohos, Rob Roser, Willis Sakumoto, Paul Simeon, Rick Tesarek, Erwin Thomas, Wayne Waldrop, and Peter Wilson. In addition, we thank the Fermilab staff and the technical staffs of the participating CDF institutions for their vital contributions. This work was supported by the US Department of Energy and National Science Foundation; the Italian Istituto Nazionale di Fisica Nucleare; the Ministry of Education, Culture, Sports, Science and Technology of Japan; the Natural Sciences and Engineering Research Council of Canada; the National Science Council of the Republic of China; the Swiss National Science Foundation; the A.P. Sloan Foundation; the Bundesministerium für Bildung und Forschung, Germany; the Korean Science and Engineering Foundation and the Korean Research Foundation; the Particle Physics and Astronomy Research Council and the Royal Society, UK; the Russian Foundation for Basic Research; the Comisión Interministerial de Ciencia y Tecnología, Spain; in part by the European Community's Human Potential Programme under contract HPRN-CT-2002-00292; the Academy of Finland; and the College of Science at Texas A&M University.

References

[1] L. Balka, et al., Nucl. Instr. and Meth. A 267 (1988) 272.
[2] M. Albrow, et al., Nucl. Instr. and Meth. A 480 (2002) 524.
[3] R. Blair, et al., CDF Collaboration, CDF II Technical Design Report, FERMILAB-Pub-96/390-E, 1996.
[4] For a more complete description of the EMTiming system as well as the most up to date reconstruction software see ⟨hepr8.physics.tamu.edu/hep/emtiming⟩.
[5] A short description of the Run I hadron calorimeter timing (HADTDC) system can be found in S. Bertolucci, et al., Nucl. Instr. and Meth. A 267 (1988) 301.
[6] There are many models of new physics that predict photons in the final state. These include S. Ambrosanio, et al., Phys. Rev. Lett. 76 (1996) 3498;
S. Dimopoulos, M. Dine, S. Raby, S. Thomas, Phys. Rev. Lett. 76 (1996) 3494;
J.L. Lopez, D.V. Nanopoulos, Mod. Phys. Lett. A 10 (1996) 2473;
S. Ambrosanio, G.L. Kane, G.D. Kribs, S. Martin, S. Mrenna, Phys. Rev. D 54 (1996) 5395;
B.C. Allenach, S. Lola, K. Sridhar, Phys. Rev. Lett. 89 (2002) 011801;
J.L. Rosner, Phys. Rev. D 55 (1997) 3143;
U. Baur, M. Spira, P.M. Zerwas, Phys. Rev. D 42 (1990) 815;
E. Boos, A. Vologdin, D. Toback, J. Gaspard, Phys. Rev. D 66 (2002) 013011;
A.D. De Rujula, M.B. Gavela, P. Hernandez, E. Masso, Nucl. Phys. B 384 (1992) 3;
M. Baillargeon, et al., hep-ph/9603220, 1996;
N. Arkani-Hamed, S. Dimopoulos, G. Dvali, Phys. Lett. B 429 (1998) 263;
A. Brignole, F. Feruglio, M.L. Mangano, F. Zwirner, Nucl. Phys. B 526 (1998) 136;
A. Brignole, F. Feruglio, M.L. Mangano, F. Zwirner, Nucl. Phys. B 582 (2000) 759;
H. Haber, G. Kane, T. Sterling, Nucl. Phys. B 161 (1979) 493;
A. Stange, W. Marciano, S. Willenbrock, Phys. Rev. D 49 (1994) 1354;
M.G. Diaz, T. Weiler, hep-ph/9401259, 1994;
A.G. Akeroyd, Phys. Lett. B 368 (1996) 89.
[7] Timing would have been very helpful for the interesting event described in F. Abe, et al. (CDF Collaboration), Phys. Rev. Lett. 81 (1998) 1791 Phys. Rev. D 59 (1999) 092002;
D. Toback, Ph.D. Dissertation, University of Chicago, 1997.

[8] D. Toback, P. Wagner, Phys. Rev. D 70 (2004) 114032.
[9] R. Erbacher, Proceedings of the 31st International Conference on High Energy Physics (ICHEP 2002), FERMILAB-CONF-02/251-E; T. Shaw, C. Nelson, T. Wesson, IEEE Trans. Nucl. Sci. NS-47 (2000) 1834.
[10] R. Moore, Proceedings of the 2004 IEEE Nuclear Science Symposium and Medical Imaging Conference, FERMILAB-CONF-04-262-E.
[11] The tracking chamber is described in T. Affolder et al., Nucl. Instr. and Meth. A 526 (2004) 249. A description of the algorithms designed to measure the collision time and z-position can be found in M. Goncharov, V. Krutelyov, D. Toback, P. Wagner, CDF Note #8015, unpublished.